

## Search for improved transparent conducting oxides: A fundamental investigation of CdO, Cd<sub>2</sub>SnO<sub>4</sub>, and Zn<sub>2</sub>SnO<sub>4</sub>

T. J. Coutts, D. L. Young, X. Li, W. P. Mulligan, and X. Wu

Citation: *Journal of Vacuum Science & Technology A* **18**, 2646 (2000); doi: 10.1116/1.1290371

View online: <http://dx.doi.org/10.1116/1.1290371>

View Table of Contents: <http://scitation.aip.org/content/avs/journal/jvsta/18/6?ver=pdfcov>

Published by the AVS: Science & Technology of Materials, Interfaces, and Processing

### Articles you may be interested in



Extracting the effective mass of electrons in transparent conductive oxide thin films using Seebeck coefficient  
*Appl. Phys. Lett.* **104**, 212103 (2014); 10.1063/1.4879995

Hydrogen-doped In<sub>2</sub>O<sub>3</sub> transparent conducting oxide films prepared by solid-phase crystallization method  
*J. Appl. Phys.* **107**, 033514 (2010); 10.1063/1.3284960

Investigation of transparent and conductive undoped Zn<sub>2</sub>In<sub>2</sub>O<sub>5-x</sub> films deposited on n-type GaN layers  
*J. Appl. Phys.* **92**, 274 (2002); 10.1063/1.1481207

Comparison of thin film and bulk forms of the transparent conducting oxide solution Cd<sub>1+x</sub>In<sub>2-2x</sub>Sn<sub>x</sub>O<sub>4</sub>  
*J. Appl. Phys.* **90**, 5979 (2001); 10.1063/1.1410882

Structural, electrical, and optical properties of transparent conductive oxide ZnO:Al films prepared by dc magnetron reactive sputtering  
*J. Vac. Sci. Technol. A* **19**, 963 (2001); 10.1116/1.1368836

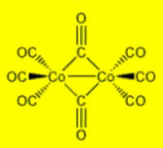
Corporate Headquarters  
Newburyport, MA USA

European Office  
Bischoffheim, France

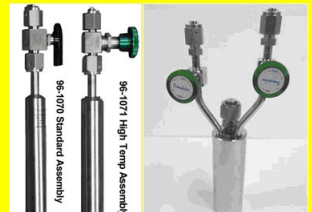
[Visit strem.com/cvd](http://strem.com/cvd)

### Over 350 CVD & ALD Precursors

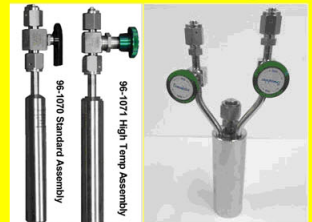
metal alkyls  
metal alkoxides  
metal β-diketonates  
volatile organometallics  
electronic grade chemicals



metal alkylamides  
metal amidinates  
volatile metal carbonyls  
fluorinated derivatives



### CVD Bubblers & ALD Cylinders



DOT and UN approved configurations available as well as precursor filling & refilling services.

## Search for improved transparent conducting oxides: A fundamental investigation of CdO, Cd<sub>2</sub>SnO<sub>4</sub>, and Zn<sub>2</sub>SnO<sub>4</sub>

T. J. Coutts,<sup>a)</sup> D. L. Young, and X. Li  
*National Renewable Energy Laboratory, Golden, Colorado 80401*

W. P. Mulligan  
*Sun Power Corporation, Sunnyvale, California 94086*

X. Wu  
*National Renewable Energy Laboratory, Golden, Colorado 80401*

(Received 10 March 2000; accepted 5 July 2000)

The bulk of developmental work on transparent conducting oxides (TCOs) has been somewhat empirical. This statement applies both to more familiar materials such as indium tin oxide (ITO) and to less-well-known materials that have emerged in recent years. In this article, we place a greater emphasis on more fundamental research. Our eventual goal is to gain a thorough understanding of these materials, their potential for further improvement, whether or not they suggest new and potentially superior materials, and the way their properties are influenced by structural and other issues. We also hope to provide guidelines to other researchers working in this area. We have investigated films of cadmium oxide (CdO), cadmium stannate (Cd<sub>2</sub>SnO<sub>4</sub> or CTO), and zinc stannate [Zn<sub>2</sub>SnO<sub>4</sub> (ZTO)]. The CdO was prepared by chemical-vapor deposition, whereas the stannates were prepared by rf sputtering. In both cases, Corning 7059 glass substrates were used. However, some depositions were also made onto tin oxide, which had a profound effect on the nucleation of CdO, in particular. It is well known that a high free-carrier mobility is essential for a TCO with near-ideal electro-optical properties. Increasing the free-carrier concentration also increases the free-carrier absorbance but a higher mobility reduces it. We have achieved free-electron mobilities in CdO ( $E_g \sim 2.4$  eV) of greater than  $200 \text{ cm}^2 \text{ V}^{-1} \text{ s}^{-1}$ , of almost  $80 \text{ cm}^2 \text{ V}^{-1} \text{ s}^{-1}$  in CTO ( $E_g \sim 3.1$  eV), but of only  $10\text{--}15 \text{ cm}^2 \text{ V}^{-1} \text{ s}^{-1}$  in ZTO ( $E_g \sim 3.6$  eV). We have characterized these materials, and will show key data, using techniques as diverse as the Nernst–Ettingshausen effect; Mössbauer, Raman, optical, and near-infrared spectroscopies; atomic-force and high-resolution electron microscopy; and x-ray diffraction. These measurements have enabled us to determine the effective mass of the free carriers and their relaxation time, the probable distributions of cations between octahedral and tetrahedral sites, the role of the deposition parameters on the carrier concentrations, and the nature of the dominant scattering mechanisms. We also consider issues relating to toxicity of cadmium and to reserves of indium. Both are of great significance to prospective large-volume manufacturers of TCO films and must be taken into account by researchers. © 2000 American Vacuum Society. [S0734-2101(00)00206-2]

### I. INTRODUCTION

#### A. Need for advanced TCOs

At some point in the near future, improved transparent conducting oxide (TCO) coatings are certain to be required for various important applications, such as thin-film photovoltaics (PVs) (Ref. 1) and flat-panel displays. Whereas the minimum resistivity reported for TCOs is typically slightly greater than  $10^{-4} \Omega \text{ cm}$ , values of perhaps half this number would benefit the applications significantly. Indeed, a value as low as this was reported by Rauf and Yuan,<sup>2</sup> but this has not been duplicated by other workers. Until recently, the electro-optical properties of the TCOs have not severely lim-

ited the performance of the flat-panel display or the PV panel. However, it has become apparent in recent years that this situation will not persist indefinitely and that there will inevitably be a need for TCOs of superior properties with the continued development of these devices. Both flat-panel displays and photovoltaic panels depend on the TCO having excellent optical transmittance across the visible range of wavelengths, as well as having excellent electrical conductivity. The TCOs are unique in nature in providing these qualities; but improving either one often worsens the other. As the areas of both types of panel/module increase, the electrical properties must also be optimized to minimize the need for, in the case of photovoltaics, scribing of the overall thin-film stack comprising the photovoltaic element, into individual subcells.<sup>3</sup>

<sup>a)</sup>Electronic mail: tim\_coutts@nrel.gov

## B. Basic properties required

It is well known that the mobility of charge carriers in a TCO thin film affects both the electrical and the optical properties.<sup>4,5</sup> To obtain high conductance and transmittance, a high mobility (greater than several  $100 \text{ cm}^2 \text{ V}^{-1} \text{ s}^{-1}$ ) is required to minimize the free-carrier absorption of near-infrared radiation. Both high mobility and carrier concentration lead to reductions in the resistivity of TCO materials. However, simply increasing the latter increases the free-carrier absorption and moves the absorption band toward the short-wavelength portion of the visible spectrum. At excessively high concentrations, this causes the familiar visual browning of the films. Therefore, increasing the mobility is the only useful option for increasing the conductivity and reducing the free-carrier absorption.

The mobility of a semiconductor is directly proportional to the carrier relaxation time and inversely proportional to the effective mass of the carriers; so the only options available are to increase the former or to decrease the latter. We may consider the former to be limited by extrinsic factors, such as a high concentration of defects in the film, which may possibly be related to film fabrication. Defects in the film can cause charge scattering that reduces the relaxation time. On the other hand, the effective mass is intrinsic to the specific semiconductor and may not be changed unless a different semiconductor is used. We assert that it is unlikely that significant improvements in the extrinsic effects will be achieved. A very large number of papers on TCOs has been published over the last three or four decades, and increases in the mobility of free carriers are not apparent in the more standard TCOs, e.g.,  $\text{SnO}_2$ , indium tin oxide (ITO), and  $\text{ZnO}$ .

These papers discuss numerous permutations of deposition methods and parameters, and we suggest that if an improvement had been possible, then it would have happened by now. That it has not yet happened suggests that it would be more fruitful to search for new TCO materials that may yield higher mobilities via either one, or both, of the intrinsic or extrinsic factors. This article discusses our approach to the problem of developing materials with much higher mobilities.

## C. Mineral reserves and cadmium toxicity

In addition to the above limitations, there is a problem with the availability of some elements involved in TCOs. Although ITO is probably the most successful of the TCOs, indium is a relatively scarce element in the earth's crust.<sup>6-9</sup> It is obtained, almost exclusively, as a by-product of zinc refining, and its estimated reserves are based on its typical abundance in zinc ores. The estimated reserves are only 2600 metric tonnes (United States Geological Survey, 1998), and the current rate of extraction is approximately 230 metric tonnes annually. Most of the indium refined is consumed in opto-electronic applications and flat-panel displays, although there is also a market for low-temperature solder involving alloys of indium. If the markets for these applications increase, as predicted, then the consumption rate of indium

will also increase. The photovoltaic industry, which serves as a useful example, has been growing at about 25% annually in recent years and is expected to continue at this rate until at least 2005. The worldwide industry presently manufactures about 200 MW annually. At the above rate of growth, this could become 760 MW by 2005. If thin-film solar cells based on copper indium diselenide provide a significant part of this requirement, or if flat-panel displays use ITO thin films, then the eventual mass of indium required could be several tens of metric tonnes annually. Given that all the output from the world's indium refineries is already consumed for other purposes, and unless we are prepared to foreshorten the life of the indium reserves by increasing refinery output, this additional demand could not readily be accommodated. We must remember that the flat-panel display industry will grow by at least this rate<sup>10</sup> and may demand even more indium. Although estimates of mineral reserves typically have a large uncertainty, the point is that the future availability of indium may be problematic. The price of indium has historically been rather volatile and has varied by as much as a factor of two within a single year.<sup>7</sup> Clearly, this presents problems for both refiners and consumers of indium. In addition, the fact that indium tin oxide has been intensively studied for many years, without showing promise for significant improvement in performance, suggests that indium-bearing compounds and alloys should not be considered as a primary element in the next-generation TCOs being considered in this article. This would not, of course, preclude them as dopants.

Precisely the same comments may be made about the development of copper indium gallium diselenide (CIGS) solar cells, in regard to both indium and gallium,<sup>7,11</sup> as well as in regard to tellurium in cadmium telluride cells.<sup>12</sup> If these devices represent a significant fraction of the future expected photovoltaics market, then further pressures on these elements will develop. However, there is little doubt that the CIGS cell will be an important first-generation product for the photovoltaics industry.<sup>13</sup> Note that selenium is also extremely limited in supply, which may limit the applicability of other semiconductor compounds and alloys.

Cadmium, like indium, derives from zinc ores. Although this article is actually concerned with cadmium-containing compounds, negative comments about these can be made on the grounds of the toxicity of cadmium.<sup>14</sup> Our purpose in developing cadmium-containing compounds is to study their fundamental properties and to attempt to determine why superior performances are associated with these, and not other, TCO compounds. Eventually, we hope to avoid both indium and cadmium in TCOs.

We have successfully developed the TCO material  $\text{Cd}_2\text{SnO}_4$  in recent years and have applied it to solar cells using  $\text{CdTe}$  as the photon absorber layer.<sup>15</sup> For this specific application, the use of cadmium may be acceptable, but only if the  $\text{CdTe}$  cell itself is acceptable to society. The quantity of cadmium in the  $\text{CdTe}$  absorber layer is far greater than that in the TCO ( $\text{Cd}_2\text{SnO}_4$ ), and the latter will not significantly affect the total amount used in a cell. Although cad-

mium is extremely toxic, primarily through the inhalation of dust, and can affect the renal and respiratory systems,<sup>14</sup> it has been claimed that its hazards, when in the form of a solar cell, may be mitigated by prior recognition and appropriate management strategies.<sup>16</sup> The cells or modules are completely encapsulated and, even in the event of a fire, would not be expected to emit significant amounts of cadmium. Careful safety analyses have been conducted that support this assertion. In addition, manufacture of CdTe solar cells has already started, thus implying that concerns are lessening.<sup>17</sup> Nevertheless, it may eventually be advisable to avoid cadmium-containing TCOs. Despite this, we are focusing on the Cd-containing compounds at present, because they perform better than alternative materials. Our study is still mainly of a fundamental nature, and we are presently attempting to determine the particular properties of cadmium compounds that seem to make them superior.

We also note that there is an imperative to work at lower deposition and processing temperatures to accommodate heat-sensitive substrates that are of great interest to flat-panel displays. Work on the development of low-temperature precursors for chemical-vapor deposition (CVD) of ZnO has already been undertaken and shows great promise and deposition of indium tin oxide films onto polyethyleneterephthalate substrates has led to films with acceptable properties. This is vital for devices based on copper indium gallium diselenide (CuInGaSe<sub>2</sub>), which depends for its operation on carefully controlled compositional gradients throughout the thickness of the absorber layer. Excessive heating can easily impair the carefully fabricated structure causing severe deterioration of device performance.

#### D. TCO activities at NREL

Our approach is mainly fundamental, but is closely related to the needs of the U.S. Department of Energy's Photovoltaic Program. To date, we have studied compounds based on the binary oxides of zinc, cadmium, and tin, as well as the spinel ternaries cadmium stannate, zinc stannate, cadmium indate, and zinc indate.<sup>18,19</sup> The former materials have relatively wide band gaps<sup>5,20–27</sup> and are already being incorporated in the CdTe solar cell, one of the front runners in the thin-film solar-cell program. We note in passing that all successful TCO materials contain a cation that has a filled *d* shell and has an electronic structure of the form  $(n-1)d^{10}ns^2$ . This point has been noted by several authors, including Zhang and Ma<sup>28</sup> and Kawazoe *et al.*<sup>29</sup> Transitions of *d* electrons would probably occur in the visible portion of the spectrum, thereby causing optical absorption.<sup>1</sup>

We have also begun to study the ternary phase field defined by the three binary oxides in the hope that a superior TCO may exist therein. We are attempting to characterize and understand the materials more thoroughly than has been done in typical investigations in recent years. Finally, we have begun a small project on the fabrication of *p*-type TCOs, these having now been demonstrated by Kawazoe *et al.*<sup>29</sup> The attraction is that it may eventually be possible to fabricate  $p^+/n^+$  tunnel junctions that could act as intercon-

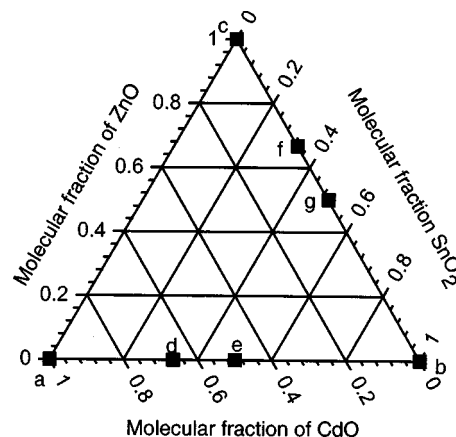


FIG. 1. Ternary phase field of the binary oxides of cadmium, tin, and zinc. The letters a, b, and c signify cadmium, tin, and zinc oxide, respectively. The letters d and f signify cadmium stannate and zinc stannate, respectively, and the letters e and g signify CdSnO<sub>3</sub> and ZnSnO<sub>3</sub>, respectively.

nects between individual cells in a tandem stack. Kudo *et al.*<sup>30</sup> successfully fabricated a *p/n* junction, but not of sufficiently heavy carrier concentration to enable tunneling to occur. For this, both sides of the junction must be degenerate. We are attempting to make CuAlO<sub>2</sub> and CuSrO<sub>2</sub>, although these aspects of the National Renewable Energy Laboratory (NREL) work will not be discussed further in this article. As suggested by some of the above comments, a host of fundamental questions exist concerning TCOs: why they work as they do, and how they may be improved to meet future demands. Some of these issues have already been discussed by Coutts *et al.*<sup>1</sup> in a meeting on basic research opportunities in photovoltaics.

## II. APPROACH

Figure 1, which illustrates the basis of our longer-term investigation, is the ternary phase diagram for the oxides of zinc, tin, and cadmium. As can be seen, to date we have investigated only the point compounds a, b, c, d, and e. We are also interested in investigating thin-film compounds that may be thermodynamically different to bulk materials, such as those studied by Kammler *et al.*<sup>31</sup> Table I shows that there is a wide variation in the properties of the three binary compounds and out-intention is to investigate a significant portion of the phase field. Given the wide variation of properties of the binary oxides, we are hopeful that there exists a ternary or quaternary compound (or alloy) with properties that are superior to Cd<sub>2</sub>SnO<sub>4</sub>. This, of course, is not guaranteed.

TABLE I. Properties of three binary TCO oxides.

Material	Crystal form	Band gap (eV)	Effective mass	Mobility (cm <sup>2</sup> s <sup>-1</sup> V <sup>-1</sup> )
ZnO	Hexagonal	3.4	0.3–0.45	~25
SnO <sub>2</sub>	Rutile	3.75	0.3	~50
CdO	Rocksalt	2.2	0.18–0.25	~220



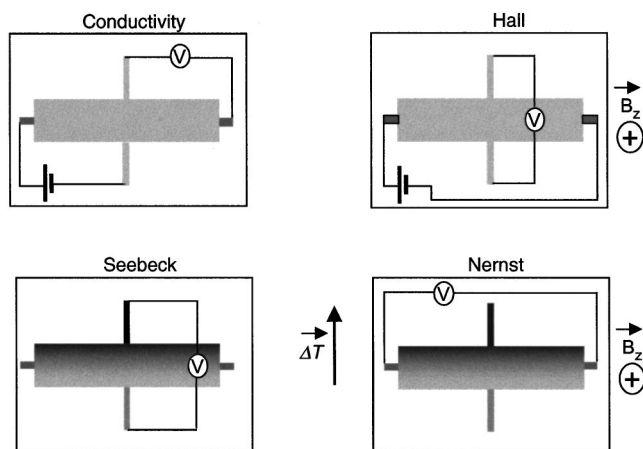


FIG. 2. Schematic of the field configurations for the four quantities measured in the *method of four coefficients*.

Of the ternary compounds,  $\text{Cd}_2\text{SnO}_4$  has proven very successful and is now being incorporated in CdTe solar cells. It may still have the potential for further improvements in resistivity, using extrinsic doping, although the effects of this on the optical properties are uncertain. Likewise,  $\text{Zn}_2\text{SnO}_4$  is also proving very useful as a high-resistance buffer layer in CdTe cells.<sup>32</sup> We are also attempting to make it more highly conducting, by optimizing the fabrication and annealing sequences.

The best-performing films of these materials are spinel in crystal form,<sup>19</sup> but we also have inadvertently made orthorhombic oriented films of  $\text{CdSnO}_3$  and  $\text{ZnSnO}_3$ . These do not perform nearly as well as the single-phase spinel films.

We made  $\text{SnO}_2$  (Ref. 33) and CdO films by CVD. However, the data for ZnO in Table I are for films made by sputtering. We plan to make all three binaries by CVD in the near future and already have potentially suitable precursors.

### III. CHARACTERIZATION TECHNIQUES

We used high-resolution electron microscopy, atomic-force microscopy, and x-ray diffraction to investigate the macroscopic properties of the films, and Raman and Mössbauer spectroscopies to investigate their microscopic properties. Raman spectroscopy has previously been employed to study  $\text{Zn}_2\text{SnO}_4$  (ZTO).<sup>34</sup> Mössbauer spectroscopy was used by Yamada *et al.*<sup>35</sup> and Williamson<sup>36</sup> to determine the role of tin in  $\text{In}_2\text{O}_3$  and by Schiessl *et al.*<sup>37</sup> to study the behavior of cations in spinel materials. These techniques, together with x-ray diffraction, enable objective comments to be made about whether the microstructure is normal or inverse spinel. In addition, we used UV/visible/IR spectrophotometry to study the optical properties.

The electrical properties were investigated using the so-called *method of four coefficients*. This method, pioneered by Kaidanov and Chernik in the 1960s,<sup>38</sup> was applied to  $p$ -PbTe crystals and enabled a determination of the effects of the heavy- and light-hole valence bands on the measured carrier mobility<sup>39</sup> to be made. The physical principles of the techniques were first defined by Kolodziejczak and Sosnowski.<sup>40</sup>

Young and co-workers<sup>41,42</sup> have applied the same technique to thin films and discuss the technique in detail, which involves simultaneous measurement of the conductivity, and Hall, Seebeck, and Nernst coefficients of a single sample. A schematic of the field configurations in each of the four measurements is given in Fig. 2. By measuring these four transport coefficients on a single sample, it is possible to determine the position of the Fermi level in relation to the conduction-band minimum (or the valence-band maximum), electron (or hole) density-of-states effective mass, relaxation time, and scattering parameter. All of these coefficients may be measured as functions of temperature. The technique provides perhaps the only method of measuring the effective mass of charge carriers in relatively disordered materials such as polycrystalline thin films. More conventional methods, such as cyclotron resonance and de Haas–Van Alphen resonance, do not work well for highly disordered films in which the electrons are typically scattered in less than the time for one cyclotron oscillation. The *method of four coefficients* depends solely on the analytical dependencies of the transport parameters on the fundamental quantities mentioned above. The mathematical principle was originally developed for materials with parabolic bands and isotropic energy surfaces, but this was generalized later to nonparabolic, anisotropic materials.<sup>43</sup> We have used both approaches in our work reported here. By measuring several samples of differing degeneracies, we were able to obtain the effective mass of the free carriers as a function of carrier concentration. This enables us to determine the shape of the conduction band (i.e., energy as a function of wave vector), up to an energy limit determined by the maximum free-carrier concentration and the associated degeneracy.

## IV. METHODS OF FILM DEPOSITION

### A. Cadmium oxide

The films of CdO were deposited in a low-pressure CVD system made by CVD Equipment Co. (Ronkonkoma, NY) and deposition could be controlled either manually or automatically. Calibrated, fast-response mass-flow controllers were used to monitor and control all gas flows. The reaction gases were introduced into the reaction chamber using four gas injectors. The typical total flow rate was in the range of 2–10 000 sccm. The chamber pressure was controlled using a throttle valve and a mechanical pump, specially enabled to handle reactive gases. The typical pressure of the chamber was 90 Torr.

The cadmium precursor was ultra-high-purity dimethylcadmium (DMCd), provided by Morton International, Inc., and it was contained in a stainless-steel bubbler. The bubbler was maintained at room temperature, at which the vapor pressure of DMCd was 30 Torr. The carrier gas was nitrogen, and the quantity of DMCd flowing to the reaction chamber was controlled via the flow rate of the nitrogen. The DMCd was mixed with oxygen directly in the reaction zone. The reaction took place in a cold-walled quartz tube, and it is expressed by

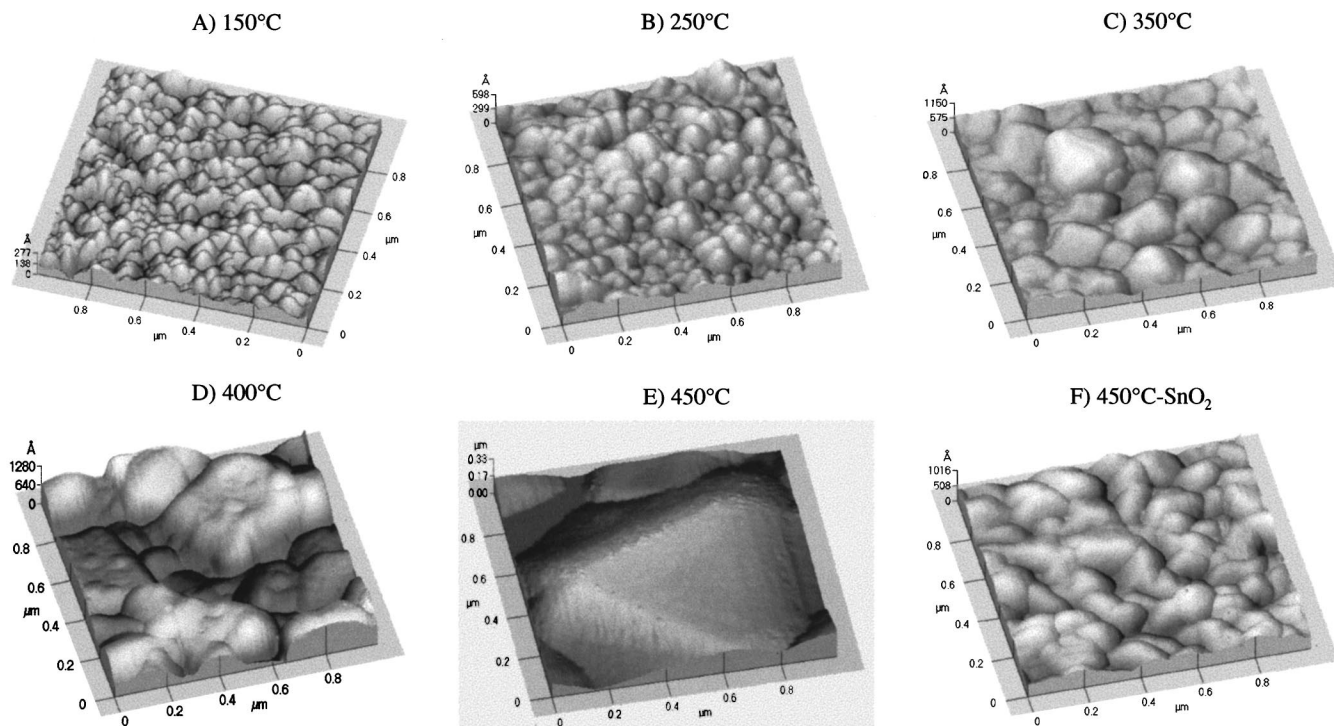
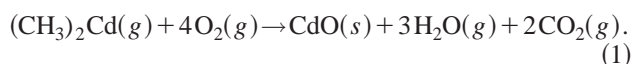


FIG. 3. Atomic-force micrographs of CdO films grown at various substrate temperatures.



The substrates were either Corning 7059 glass or single-crystal silicon wafers, and they were arranged horizontally on a graphite susceptor. There was a pocket, machined in the susceptor, that was 1 mm deep, 306 mm long (in the direction of the gas flow), and 102 mm wide. The susceptor could support three silicon wafers of 102 mm diam, or four 7059 substrates of 76 mm×76 mm. Films were deposited at various temperatures in the range of 150–450 °C with oxygen flow rates of 400–10 000 sccm. The substrate temperature and oxygen flow rate determined the growth rate, and film thicknesses were in the range of 50–500 nm.

### B. Cadmium stannate and zinc stannate

Films of  $\text{Cd}_2\text{SnO}_4$  were made by radio-frequency (rf) sputtering; the details of the deposition parameters are given by Wu, Mulligan, and Coutts.<sup>44</sup> We previously determined that the optimum electro-optical properties of  $\text{Cd}_2\text{SnO}_4$  were obtained when the films were deposited in pure oxygen onto substrates that were nominally at room temperature. The films were subsequently annealed at various temperatures up to 680 °C. This procedure resulted in single-phase spinel structures. The carrier concentrations were as high as  $7\text{--}9 \times 10^{20} \text{ cm}^{-3}$ , with mobilities as high as  $68 \text{ cm}^2 \text{ V}^{-1} \text{ s}^{-1}$ . The optical properties of these films were also excellent, as expected from the relatively high mobilities.

Films of  $\text{Zn}_2\text{SnO}_4$  were also made by rf sputtering, but the optimum deposition parameters have not yet been determined. Consequently, a number of combinations have been

used. These include: room-temperature deposition in oxygen, forming gas or argon followed by annealing at various temperatures, up to 680 °C, in argon, forming gas, oxygen, air, and vacuum. Although earlier work produced single-phase spinel  $\text{Zn}_2\text{SnO}_4$ ,<sup>19</sup> the best films in the present work were amorphous, with carrier concentrations up to  $2 \times 10^{19} \text{ cm}^{-3}$  and mobilities in the range  $10\text{--}15 \text{ cm}^2 \text{ V}^{-1} \text{ s}^{-1}$ .

## V. RESULTS

### A. Cadmium oxide

Figures 3(a)–3(f) show a sequence of atomic-force micrographs (AFMs) of CdO films deposited at a series of substrate temperatures. In each case, the area shown is  $1 \mu\text{m} \times 1 \mu\text{m}$  and the deposition temperature ranged from 150–450 °C. Clearly, there is a systematic growth of the grains with substrate temperature until, for the film deposited 450 °C, a single grain occupies essentially the entire field of view. This is a single grain in a film that was not continuous. However, when the CdO was deposited onto a glass substrate precoated with a layer of  $\text{SnO}_2$ , the grain size was greatly reduced and electrical continuity was maintained. Figure 4 shows the root-mean-square (rms) roughness and grain size for the same temperatures used in Fig. 3. These data were also obtained from AFM. From Figs. 3(a)–3(f) and 4, it is clear that the grains grow three-dimensionally with increasing substrate temperature. The film thicknesses lay between 57.2 and 80.0 nm, and the roughness was, therefore, a significant proportion of the latter. Figure 4 also shows the rms roughness of a CdO film that was deposited on a

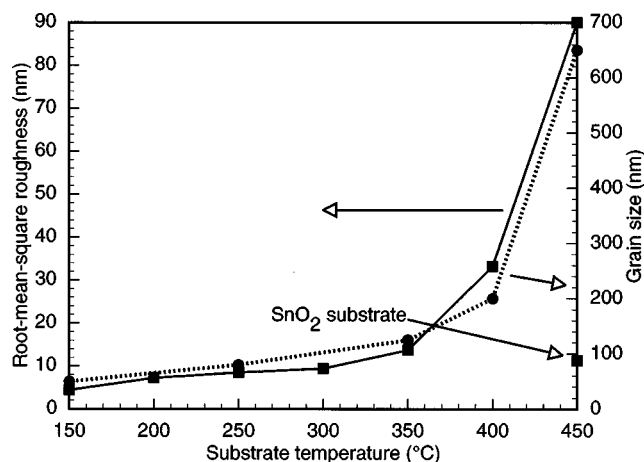


FIG. 4. Root-mean-square (rms) roughness and grain size of cadmium oxide films grown at various substrate temperatures.

$\text{SnO}_2$ -coated substrate. This film has a much lower roughness, corresponding to the much smaller grain size, illustrated in Fig. 3(f).

Figures 5(a)–5(f) show x-ray diffraction (XRD) spectra of the same set of CdO films shown in the previous two figures. In going from the film deposited at 250 °C to that at 350 °C, there is clearly a very large change in the structure of the film. First, the (111) peak, which had dominated the two lower temperatures, disappears at 350 °C and is replaced by a strong (200) peak. For substrate temperatures of 350 °C and greater, there is clearly a preferred orientation, which may be confirmed by comparison with the American Society

for Testing and Materials (ASTM) reference spectra. The film deposited at 450 °C onto a  $\text{SnO}_2$ -coated substrate is shown in Fig. 5(f). The crystal structure of the film deposited on the coated substrate is more like that of the film deposited on glass at 250 °C. This is consistent with Figs. 3 and 4. The broad maximum for  $2\theta \sim 25^\circ$  is due to the glass substrate and could be eliminated by a subtractive process.

Figure 6 shows a high-resolution transmission electron micrograph (TEM) of a CdO film deposited at 450 °C. As with the previous films discussed in this section, the film was deposited by CVD and was well oriented. The size of the image was  $\sim 50 \text{ nm} \times 50 \text{ nm}$ . The most striking feature was that lattice fringes running from top left to bottom right are clearly visible, indicating that the film is of high quality. In itself, this would lead us to expect excellent electron-transport properties.

In Fig. 7, we show the variation of carrier concentration (left-hand y axis) and mobility (right-hand y axis) as functions of deposition temperature. In this, it can be seen that the mobility increases rapidly with substrate temperature, up to a maximum of  $220 \text{ cm}^2 \text{ V}^{-1} \text{ s}^{-1}$ . To our knowledge, this is the highest mobility ever recorded for CdO, although values in excess of  $100 \text{ cm}^2 \text{ V}^{-1} \text{ s}^{-1}$  have been observed.<sup>45</sup> In bulk form (sintered powders), values of mobility of greater than  $200 \text{ cm}^2 \text{ V}^{-1} \text{ s}^{-1}$  have been observed, although this is not true in the case of thin films.<sup>46</sup> Although the mobility increases with substrate temperature, the carrier concentration decreases even more rapidly; and although values in excess of  $10^{21} \text{ cm}^{-3}$  are found for low-temperature depositions, the concentration decreases to as low as  $10^{19} \text{ cm}^{-3}$  at

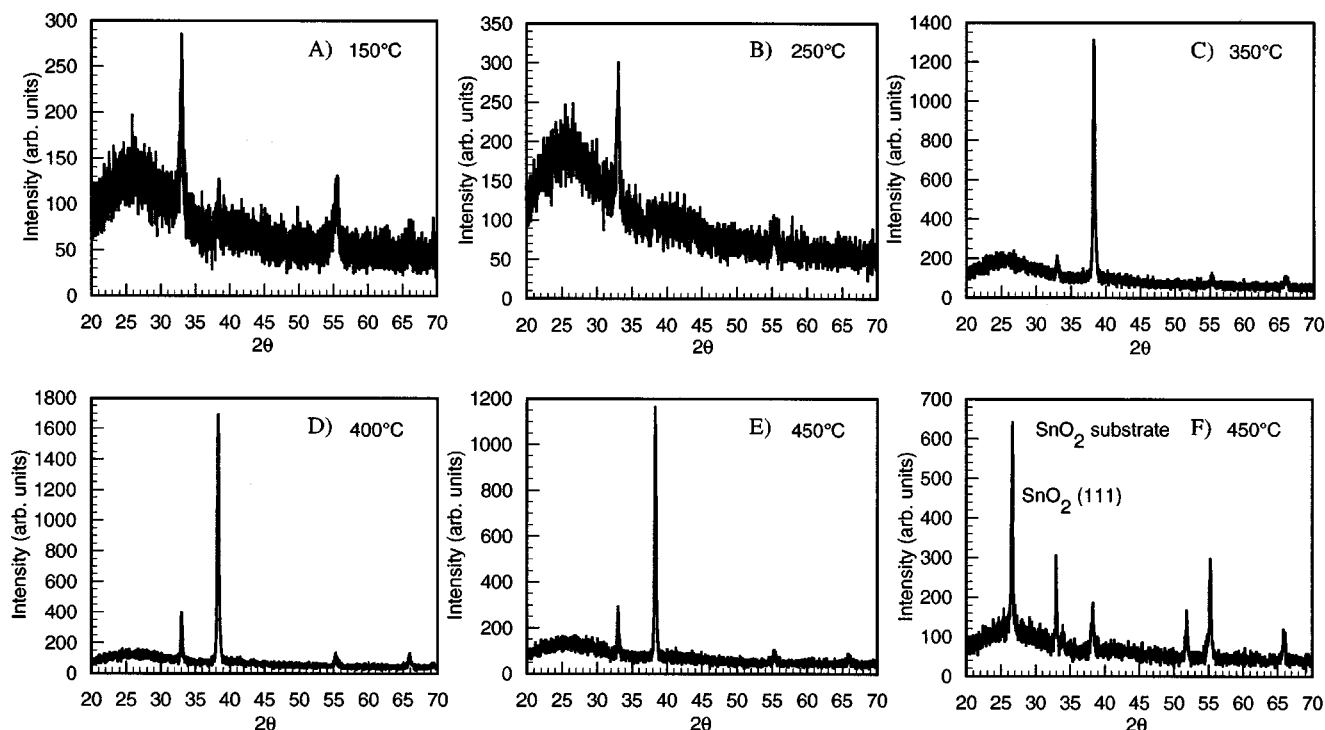


FIG. 5. X-ray diffraction spectra of the same sequence of films shown in Fig. 3.





FIG. 6. High-resolution transmission electron micrograph of a film of CdO.

higher temperatures. The consequences of this is that the minimum resistivity for this sequence was slightly less than  $2 \times 10^{-3} \Omega \text{ cm}$ , which is more than one order of magnitude too high for device applications. Nevertheless, it has been established that CdO, one corner point of the ternary phase diagram discussed earlier, has good transport properties.

Figure 8 shows the variation of the Seebeck (left-hand y-axis) and Nernst (right-hand y-axis) coefficients of CdO films as functions of  $n^{-2/3}$ . The lines are used merely to connect the points, and have no physical significance. For a parabolic conduction band, theory predicts that the coefficients should be linear with  $n^{-2/3}$ . The data in Fig. 8 show that this is not the case for CdO, thereby implying that the conduction band is nonparabolic, which is supported by the nonlinearity in the Nernst coefficient. Notice that the sign of the Nernst coefficient changes and becomes negative at

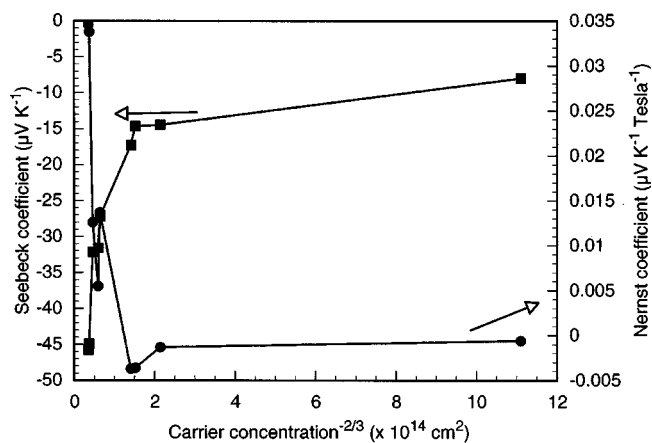


FIG. 8. Variation of the Seebeck and Nernst coefficients of CdO films with carrier concentration.

higher carrier concentrations. This suggests that there is a change in the charge-carrier scattering mechanism with carrier concentration, as has been observed for bulk samples of CdO (Ref. 47) and for films of  $\text{Cd}_2\text{SnO}_4$ .

It is possible to generalize transport theory to accommodate nonparabolic conduction bands and to include materials that are nonisotropic in  $k$  space. Young *et al.*<sup>40</sup> applied this technique to ZnO, and it was used in the present work to analyze the transport properties of electrons in CdO. Figure 9 illustrates this and shows that the effective mass (left-hand y axis) increases approximately linearly with increasing carrier concentration, from a value of  $\sim 0.14 m_e$  to a value of  $\sim 0.3 m_e$  over the range of carrier concentrations investigated, in agreement with measurements on bulk samples.<sup>48</sup> This confirms that the conduction band is nonparabolic. The carrier relaxation time is shown on the right-hand y axis of Fig. 9. This quantity decreases strongly with increasing carrier concentration. At low carrier concentrations, the relaxation time is long ( $\sim 2 \times 10^{-14} \text{ s}$ ) and the effective mass is small ( $\sim 0.14 m_e$ ). These effects are responsible for the extraordinarily high mobility (for a TCO), shown in Fig. 7. As the

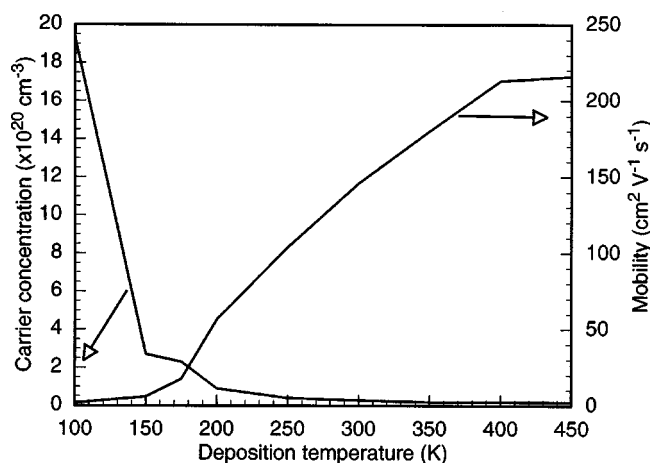


FIG. 7. Variation of carrier concentration (left-hand y axis) and mobility with growth temperature.

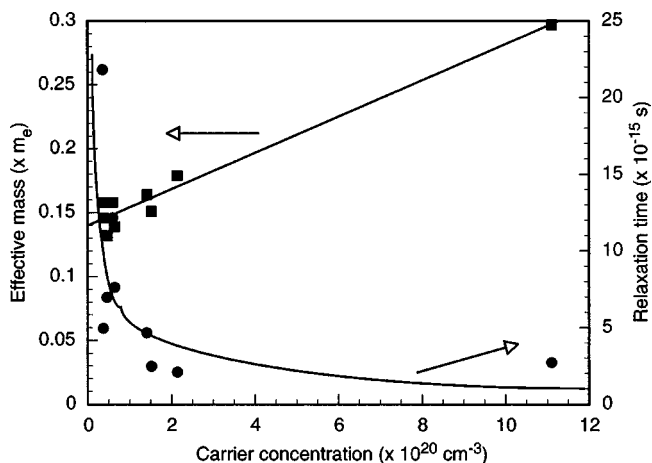


FIG. 9. Variation of the effective mass and relaxation time of CdO films with carrier concentration.



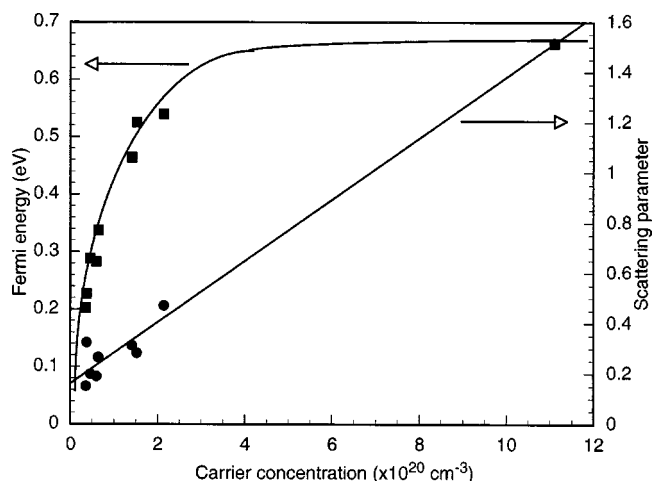


FIG. 10. Variation of the Fermi energy and scattering parameter of CdO films with carrier concentration.

carrier concentration increases, the effective mass increases by a factor of 2, while the relaxation time decreases by  $\sim 1$  order of magnitude. Caution must be exercised in the interpretation of these data in view of the fact that there is a progressive change in crystal structure with deposition temperature.

Figure 10 shows the variation of the scattering parameter (right-hand y axis) and the Fermi level (left-hand axis) with carrier concentration.  $s'$  relates the relaxation time to the Fermi energy ( $\tau \alpha E_F^{s'}$ ), and it gives an indication of the mechanism(s) of electron scattering. Different values of  $s'$  signify specific scattering mechanisms. A value of  $s' = 3/2$ , for example, implies ionized impurity scattering, whereas  $s' = 1/2$  implies that optical phonons are responsible for scattering the electrons. For CdO thin films, as Fig. 10 shows, the former mechanisms apply at the upper and lower limits, respectively, of the range of carrier concentrations investigated, and they have previously been suggested for bulk materials, but not for thin films.<sup>47</sup> Note that the Fermi level, measured with respect to the conduction-band minimum, is approximately 0.6 eV. In calculating the data for Fig. 10, we have taken into account the fact that the conduction band is nonparabolic, as evidenced by the increasing value of the effective mass with carrier concentration.

In this section, we have shown that CVD of CdO from a  $\text{Cd}(\text{CH}_3)_2$  precursor leads to high-quality, well-oriented films consisting of large crystallites. The mobility is high at low carrier concentrations because of a long relaxation time and a low effective mass. It has not yet been possible to obtain both high mobilities and carrier concentrations. The conduction band is clearly nonparabolic, and the mechanism of charge scattering changes with increasing carrier concentration.<sup>47</sup>

## B. Cadmium stannate

Bulk cadmium stannate ( $\text{Cd}_2\text{SnO}_4$ ) may be either orthorhombic or spinel,<sup>49</sup> depending on fabrication conditions. However, the orthorhombic form is the more stable

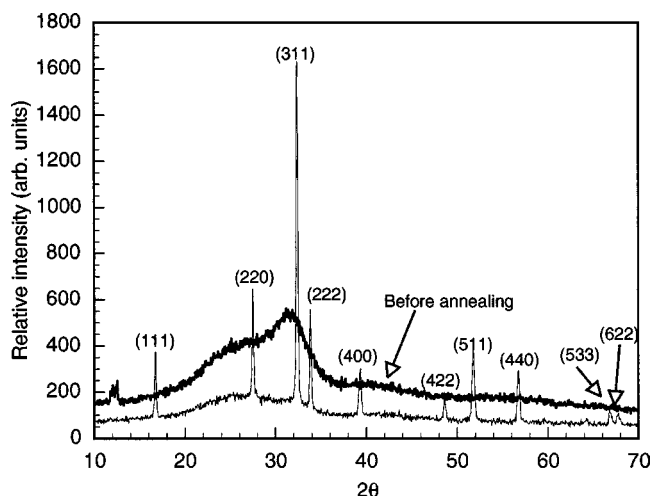
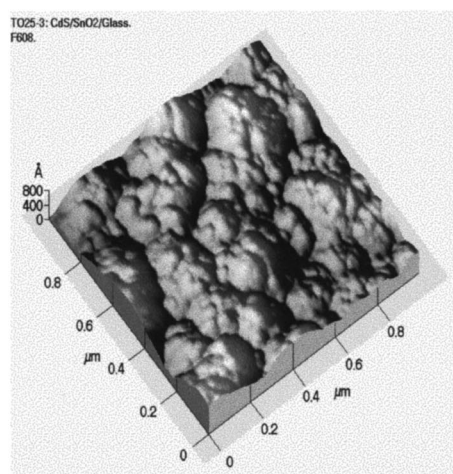


FIG. 11. XRD spectra of  $\text{Cd}_2\text{SnO}_4$  before and after annealing (see Ref. 5).

thermodynamically.<sup>31</sup> We have previously found that sputtering targets are orthorhombic, but annealed thin films are spinel. The spinel unit cell is essentially a close-packed array of oxygen atoms, with cadmium and tin ions located at the interstices between the planes of oxygen atoms. Spinel ( $\text{MgAl}_2\text{O}_4$ ) occurs naturally, and many different chemical variants have been identified.<sup>50</sup> In  $\text{Cd}_2\text{SnO}_4$ , the cadmium ions (in principle) are surrounded by six oxygen atoms, i.e., the cadmium is octahedrally coordinated, whereas the tin atoms are located at the geometrical center of oxygen tetrahedra. There are twice as many cadmium octahedra as tin tetrahedra, and the unit cell contains 56 atoms. The symmetries for the tetrahedral and octahedral sites are cubic and trigonal, respectively. When the tin ions change position from cubic to trigonal symmetry, they experience a change in the electric-field environment and this causes the Mössbauer quadrupole splitting. Note that spinel structures are based on combinations of group II/group IV, as well as group II/group III, atoms.  $\text{CdIn}_2\text{O}_4$ , for example, was investigated by Wu, Coutts, and Mulligan<sup>19</sup> as a potential TCO.

The  $\text{Cd}_2\text{SnO}_4$  unit cell, as described above, is referred to as “normal.” However, it is also possible for an exchange between the cadmium and tin ions to take place. If the tin ions are located at half of the octahedral sites, and half of the cadmium ions are located at the tetrahedral sites, then the structure is described as “inverse.” It is also possible to obtain mixtures of the normal and inverse forms. These issues may be relevant to the origins of free carriers in the films, which have not yet been extrinsically doped. It has, however, been observed that  $\text{Cd}_2\text{SnO}_4$  films tend to be cadmium deficient (possibly because of the volatility of cadmium), and Mulligan<sup>51</sup> suggested that a substitutional doping mechanism, involving tin on cadmium vacancies, could cause the relatively high carrier concentrations observed in  $\text{Cd}_2\text{SnO}_4$ . It is believed that zinc stannate ( $\text{Zn}_2\text{SnO}_4$ ) behaves very similarly to  $\text{Cd}_2\text{SnO}_4$  and typically exists in the inverse form. Electrically, however, it has exhibited a much lower carrier concentration and mobility than  $\text{Cd}_2\text{SnO}_4$ , to

## Tin oxide



## Cadmium stannate

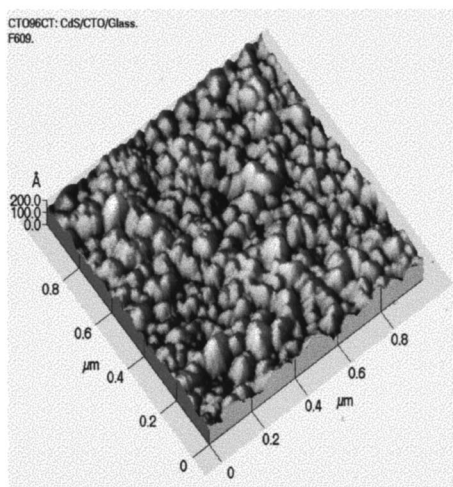


FIG. 12. AFMs of  $\text{SnO}_2$  and  $\text{Cd}_2\text{SnO}_4$  (see Ref. 5).

date, and one of our objectives is to fabricate lower resistivity material.

Figure 11 shows XRD spectra of  $\text{Cd}_2\text{SnO}_4$  before and after annealing. This result was first presented by Coutts *et al.*<sup>5</sup> The as-deposited films were amorphous before annealing, but they crystallized in the spinel form after annealing in close proximity to a film of CdS that had been deposited by chemical-bath deposition. The annealing temperature was 660 °C, and the film had been deposited in pure oxygen, nominally at room temperature. After annealing, it can be seen that substantial crystallization had taken place, and the indexed peaks correspond to those shown in the ASTM database. We have also previously established that a single-phase film (such as that shown here) is essential for high-quality films with excellent electron-transport and optical properties.

Figure 12 shows atomic-force micrographs of  $\text{SnO}_2$  and  $\text{Cd}_2\text{SnO}_4$  films. In both cases, the area examined is  $1\text{ }\mu\text{m} \times 1\text{ }\mu\text{m}$ . The latter had been annealed as described earlier. The rms roughness of the tin oxide film was about  $\pm 12.6\text{ nm}$ , whereas that of the  $\text{Cd}_2\text{SnO}_4$  was only  $\pm 3.2\text{ nm}$ . Wu *et al.*<sup>32</sup> discussed the importance of this minimal roughness for cadmium telluride solar cells. The  $\text{Cd}_2\text{SnO}_4$  films also have superior mobility (with values of almost  $80\text{ cm}^2\text{ V}^{-1}\text{ s}^{-1}$ ), leading to one of the lowest TCO resistivities ever recorded and minimal free-carrier absorbance.<sup>5</sup>

Figure 13 shows a TEM of a region of an annealed film of  $\text{Cd}_2\text{SnO}_4$ , the area shown being about  $30\text{ nm} \times 30\text{ nm}$ . Once again, lattice fringes can clearly be seen, indicating that the fabrication procedures used led to excellent-quality material after annealing. The regions in the top left and right of the diagram show additional crystallites, with discontinuities at the grain being evident. Towards the bottom left and right of the diagram, regions that appear to be amorphous in structure are evident. Nevertheless, the extent of the fringes indicates that there is a high degree of perfection within individual grains of material.

Figure 14 shows the Seebeck (left-hand y-axis) and Nernst (right-hand y-axis) coefficients as functions of carrier

concentration. The straight lines are least-squares fits and, to a reasonable approximation, they are linear with  $n^{-2/3}$ , thereby demonstrating that the conduction band is parabolic over the range of carrier concentrations investigated. Notice that the Nernst coefficient is, once again, positive at low carrier concentrations and negative at high values. Consequently, we believe that the scattering mechanism changes with carrier concentration.

Figure 15 shows the Fermi energy of  $\text{Cd}_2\text{SnO}_4$  as a function of carrier concentration. The Fermi energy is measured with respect to the conduction-band minimum, and it can be seen that at the highest carrier concentrations ( $\sim 7 \times 10^{20}\text{ cm}^{-3}$ ) the degeneracy is almost 1 eV. Hence, even though the fundamental energy gap of  $\text{Cd}_2\text{SnO}_4$ , may be too small for a high-performance TCO, with the large degeneracy, the optical gap ( $E_g + \Delta E_g$ ) becomes at least as wide as those of more conventional TCOs.

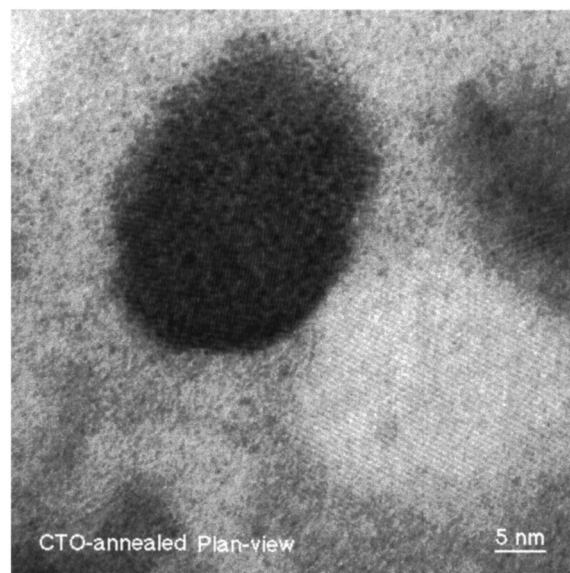


FIG. 13. Grain of  $\text{Cd}_2\text{SnO}_4$  for an annealed film.

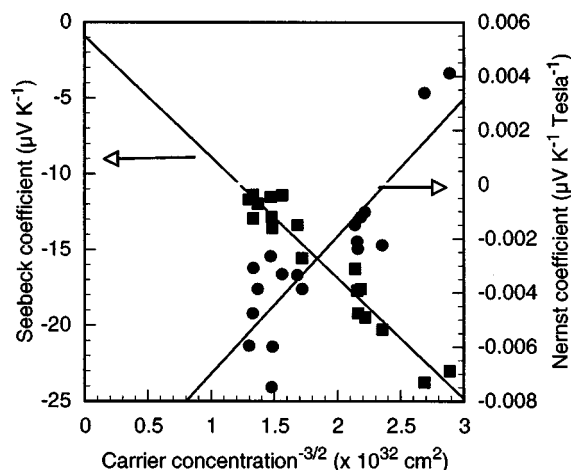


FIG. 14. Seebeck (left-hand y axis) and Nernst (right-hand y axis) coefficients as functions of carrier concentration.

Figure 16 shows the effective mass (left-hand y axis) and scattering parameter (right-hand y axis) as functions of carrier concentration in the range discussed previously. The values of effective mass are constant to within the experimental uncertainty ( $\pm 0.025 m_e$ ) estimated for the *method of four coefficients*. The linearity of the Seebeck and Nernst linearities with  $n^{-2/3}$  suggested that this would be the case. At high carrier concentrations, the Nernst coefficient is negative, but for the few very low concentration films, it is positive. The changing scattering parameter with carrier concentration follows the same general trend as that observed for cadmium oxide.

Figure 17 shows the Mössbauer spectrum of a film of  $\text{Cd}_2\text{SnO}_4$ . This film was deposited on stainless steel and was annealed at  $660^\circ\text{C}$ . The measurement was made using a 2 m Curie source of  $^{119}\text{Sn}$ , and the spectrum was taken over a period of several hours. The fact that there is no isomer shift indicates that the tin is in the  $\text{Sn}^{4+}$  state. The spectroscopy depends on the homogeneity of the electric field within the films due to individual ions. The dotted data show the actual

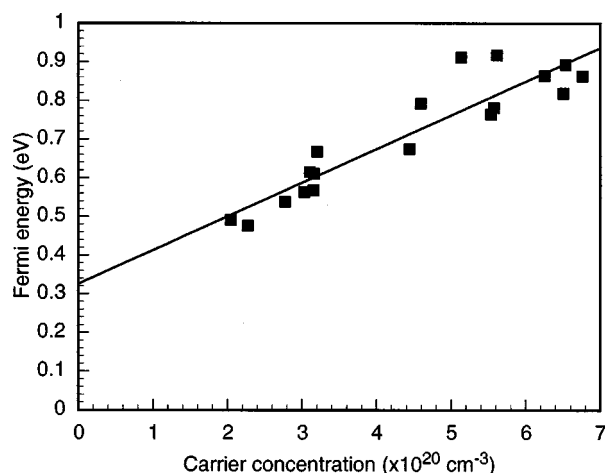


FIG. 15. Variation of the Fermi energy of  $\text{Cd}_2\text{SnO}_4$  with carrier concentration.

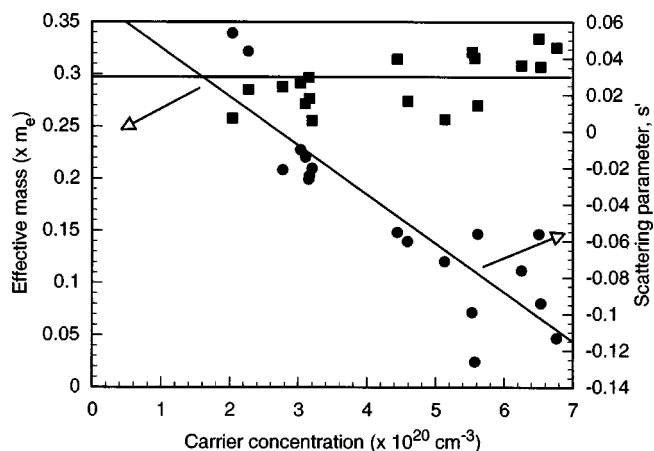


FIG. 16. Variation of effective mass (left-hand y axis) and scattering parameter of  $\text{Cd}_2\text{SnO}_4$  films as a function of carrier concentration.

measurements (made in collaboration with the Colorado School of Mines), and the solid curve shows the “best fit” to the data. The data were fitted satisfactorily using a Lorentzian doublet and singlet. The goodness of fit was excellent, and the statistics indicated that 39% of the singlet peak and 61% of the doublet peak gave the best fit. A normal spinel would not exhibit quadrupole splitting, whereas there is slight evidence of quadrupole splitting, which is a strong indication of the formation of the inverse spinel phase. This is in good agreement with the observations of Shannon<sup>52</sup> who found his data were best represented by 65% of the cadmium being in the tetrahedral site (the doublet), with 35% of the tin also being in this location (the singlet). We are not yet fully convinced that the film material is in the inverse form and further experiments are being performed to clarify this matter. However, if the inverse spinel is formed, then a possible explanation of self-doping may be provided.

In Fig. 18, we show the variation of reflectance, transmittance, and absorbance as functions of wavelength for a single film with a carrier concentration of  $5 \times 10^{20} \text{ cm}^{-3}$ . The data show measured and modeled data and, as can be seen, the

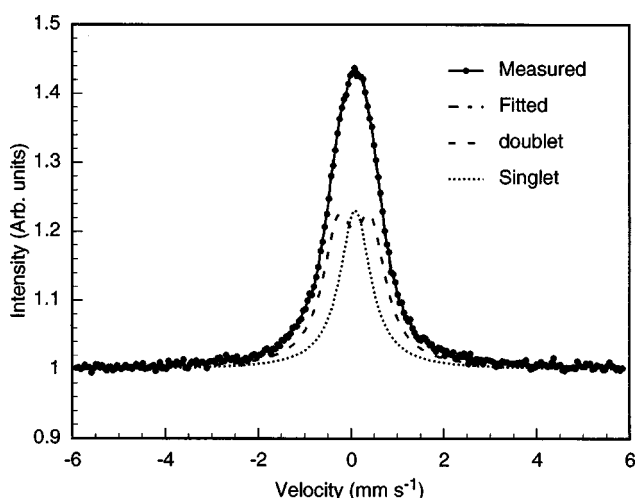


FIG. 17. Mössbauer spectrum of a film of  $\text{Cd}_2\text{SnO}_4$ .



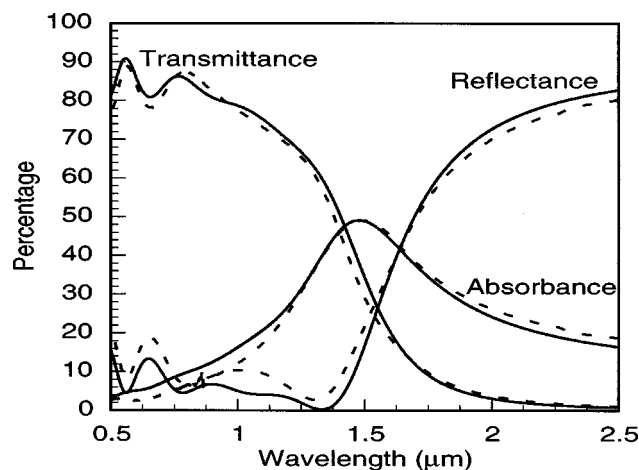


FIG. 18. Measured and modeled reflectance, transmittance, and absorbance of a  $\text{Cd}_2\text{SnO}_4$  film as functions of wavelength.

agreement between each pair (in particular, the transmittance data) is excellent. The model data were obtained using the software package TFCALC 3.3, obtained from Software Spectra, Inc. The optical properties are particularly well behaved, and the three parameters that are output from the model gave  $m^* \sim 0.3m_e$ , a relaxation time of about  $10^{-14}$  s, and an optical mobility (for this particular film) of  $60 \text{ cm}^2 \text{ V}^{-1} \text{ s}^{-1}$ . The value of the effective mass is very close to the values obtained using the *method of four coefficients*, shown in Fig. 16. This result has further implications that will be discussed later. The optical modeling package takes transmittance and/or reflectance data and performs a “best fit” to these. The film thickness may be used as an input to the model, or it may be treated as one of the adjustable parameters and obtained as an output. In general, the procedure outputs three parameters: the first gives the high-frequency permittivity, the second gives the effective mass, and the third gives the relaxation time. The software is based strictly on the Drude model and with these three output quantities, it is possible to obtain the real and imaginary parts of the refractive index. These quantities are shown in Fig. 19 and they are typical of

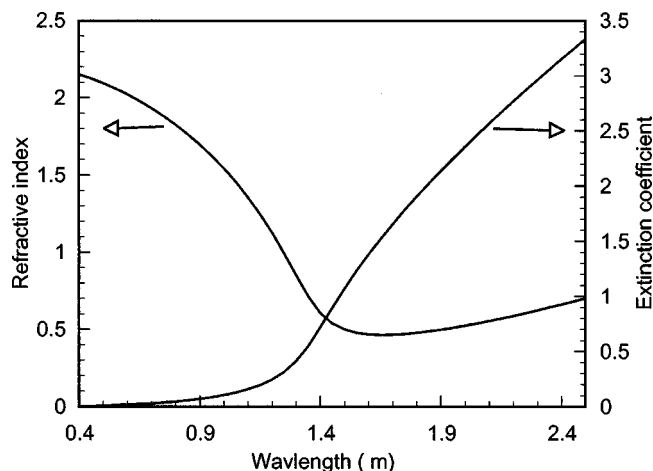


FIG. 19. Real and imaginary parts of the refractive index of  $\text{Cd}_2\text{SnO}_4$ .

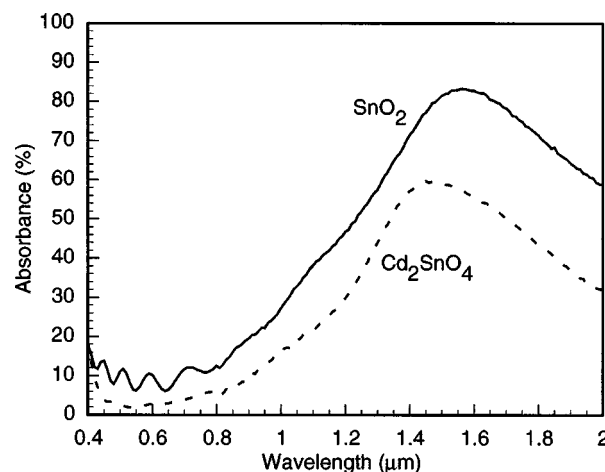


FIG. 20. Free-carrier absorbance of films of  $\text{Cd}_2\text{SnO}_4$  and  $\text{SnO}_2$  (see Ref. 19).

free-electron-dominated materials that follow the Drude model. The imaginary part of the refractive index is near zero at higher frequencies and increases rapidly at a specific wavelength that is approximately equal to the plasma wavelength.

The peak of the free-carrier absorbance curve of a film of  $\text{Cd}_2\text{SnO}_4$ , although still as high as 50%, is significantly less than that of a film of commercially available  $\text{SnO}_2$ , as shown in Fig. 20.<sup>15</sup> Although the thickness and carrier concentration of the  $\text{SnO}_2$  are slightly less than that of the latter, the improved optical quality is due primarily to the greatly increased carrier mobility. Consequently,  $\text{Cd}_2\text{SnO}_4$  is now sometimes used as the transparent electrode in CdTe solar cells, rather than the more-common  $\text{SnO}_2$ .

In summary, within the range of carrier concentrations studied ( $2-7 \times 10^{20} \text{ cm}^{-3}$ ), the conduction band is parabolic to within experimental uncertainty. Mobilities as high as  $80 \text{ cm}^2 \text{ V}^{-1} \text{ s}^{-1}$  have been recorded, probably because of the high degree of structural order indicated by high-resolution electron microscopy. Mössbauer spectroscopy indicates that the  $\text{Cd}_2\text{SnO}_4$  films are either mixed normal/inverse phases, or, more simply, pure inverse spinel.

Modeling of the Seebeck coefficient shows that the scattering mechanism is due to optical phonons at high carrier concentrations and is intermediate between optical phonons and neutral impurities at low concentrations. The optical properties follow the Drude model well, and the optical mobility is approximately equal to that derived from the *method of four coefficients*.

### C. Zinc stannate

Zinc stannate ( $\text{Zn}_2\text{SnO}_4$ ) films were deposited by rf sputtering in the same way as the  $\text{Cd}_2\text{SnO}_4$  (CTO) films. However, a different annealing sequence has been used and had not been optimized at the time of writing. Figure 21 shows a high-resolution transmission electron micrograph of an “as-deposited” zinc stannate film. This film had been deposited onto a silicon substrate in an atmosphere of argon, and the



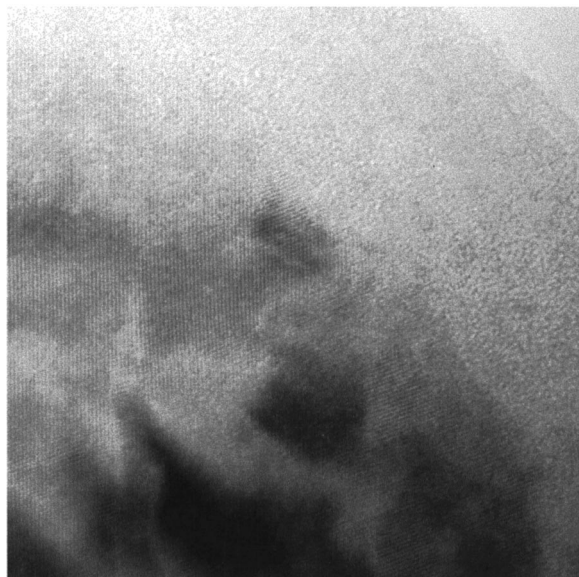


FIG. 21. High-resolution transmission electron micrographs of an "as-deposited"  $\text{Zn}_2\text{SnO}_4$  film.

film had not been annealed. The size of the image shown is  $\sim 30 \text{ nm} \times 30 \text{ nm}$ . Figure 21 provides a striking contrast with the earlier micrographs of CdO and  $\text{Cd}_2\text{SnO}_4$ . Individual lattice fringes do not extend unbroken across the entire field of view, as was the case of the latter films. Rather, individual lattice fringes in various directions can be seen, as well as an apparently amorphous region in the top right and lower right of Fig. 21. This indicates that the structure of the films had not yet been optimized, either during or after deposition.

Figure 22 shows a Mössbauer spectrograph of a zinc stannate film. Previous authors have also used this technique to determine whether ZTO and CTO are in the normal or inverse forms.<sup>34</sup> The dotted data show the actual measurements (made in collaboration with the Colorado School of Mines), and the solid curve shows the "best fit" to the data. As can

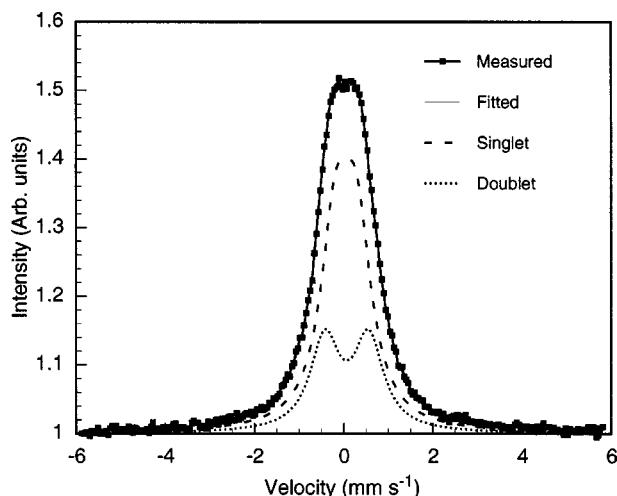


FIG. 22. Mössbauer spectrograph of a  $\text{Zn}_2\text{SnO}_4$  film.

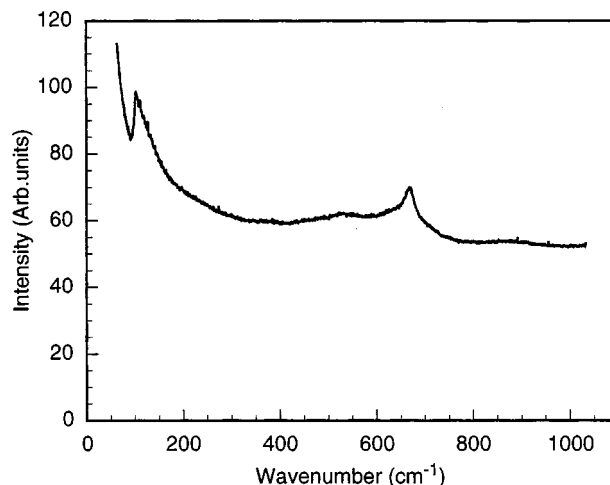


FIG. 23. Raman spectrum of a  $\text{Zn}_2\text{SnO}_4$  film.

be seen, there is again evidence of quadrupole splitting, indicating formation of the inverse spinel phase. XRD integrated intensity ratios confirm this.

Figure 23 shows a Raman spectrum of an annealed ZTO film. This film was grown on a stainless-steel substrate, to avoid overlap of peaks, and it was measured with a laser wavelength of 514.5 nm. The strong peak at  $666.6 \text{ cm}^{-1}$  corresponds to a known ZTO peak. The absence of the other four Raman peaks may indicate the poor crystallinity of the film. This suggestion is further supported by the presence of a strong amorphous peak in the XRD spectrum.

At present, the mobilities of  $\text{Zn}_2\text{SnO}_4$  have been comparatively modest ( $< 20 \text{ cm}^2 \text{ V}^{-1} \text{ s}^{-1}$ ) but, as Fig. 21 showed, the crystallization of the films is far from complete. The carrier concentrations have also been rather low to date ( $10^{18} - 10^{19} \text{ cm}^{-3}$ ), and we are investigating means of increasing this quantity. Transport measurements of the only crystalline ZTO made to date give an effective mass of  $0.1 m_e$  and a short relaxation time of  $8 \times 10^{-16} \text{ s}$ . This is almost certainly associated with the poor crystallinity of the material. Hence, we believe that it may still be possible to produce high-quality ZTO with much higher mobilities, by appropriate growth or annealing procedures.

## VI. DISCUSSION

### A. Cadmium oxide

Although CdO has a relatively low fundamental band gap, the electrons have a low effective mass, which causes the Fermi level to increase in energy rapidly with carrier concentration. Our data show that CdO can be made with a degeneracy of more than 1 eV, causing the optical gap (the energy for a transition from the valence-band maximum to the Fermi energy) to be greater than 3 eV. At this level, it could be regarded as a potentially useful TCO. CdO has a nonparabolic conduction band, as assessed by the *method of four coefficients*. We have achieved unusually high electron mobilities at low carrier concentration. This appears to be due to the high degree of structural perfection, leading to a long

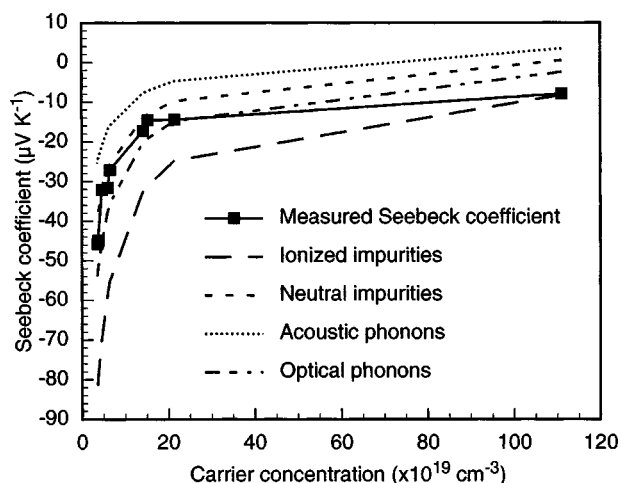


FIG. 24. Solid squares indicate the variation of the Seebeck coefficient of CdO with carrier concentration. The various dashed lines show the modeled variation, as determined by several possible scattering mechanisms.

carrier relaxation time. The mobility decreases rapidly when the carrier concentration increases because the effective mass increases. These mutually dependent changes lead to the minimum resistivity being limited to  $2 \times 10^{-3} \Omega \text{ cm}$ . The effective mass increases approximately linearly with carrier concentration.

We modeled the variation of the Seebeck coefficient with carrier concentration for neutral and ionized impurities, as well as for acoustic and optical phonons. The modeled and measured data are shown in Fig. 24. At low carrier concentrations, it is difficult to be unambiguous about the nature of the scattering process because the measured and modeled values of the Seebeck coefficient vary rapidly with carrier concentration. Nevertheless, up to a carrier concentration of about  $2 \times 10^{20} \text{ cm}^{-3}$ , it appears that neutral impurity scattering gives the best fit to the data. Unfortunately, there are very few data between  $2 \times 10^{20} \text{ cm}^{-3}$  and the highest carrier concentration of about  $1.1 \times 10^{21} \text{ cm}^{-3}$ . However, for the highest carrier concentration, ionized impurities give the best fit to the measured data. Hence, it is reasonable to say that the charge-carrier scattering mechanism changes with carrier concentration, with either optical phonons or neutral impurities being dominant at low concentrations and with ionized impurities being the scattering centers at high concentrations.

The CdO films are nominally undoped, and the source of the electrons has not yet been resolved. Although Cd interstitials and oxygen vacancies have both been suggested as the source of the carriers, in view of the fact that we use metal-organic CVD to deposit the films, we must also consider carbon as an impurity that may be electrically active. Further work is needed to clarify the source of the carriers.

## B. Cadmium stannate

We have also analyzed films of  $\text{Cd}_2\text{SnO}_4$  in detail. The conduction band of this material is parabolic over the range of carrier concentrations investigated. The effective mass of the electrons does not appear to be significantly lower than

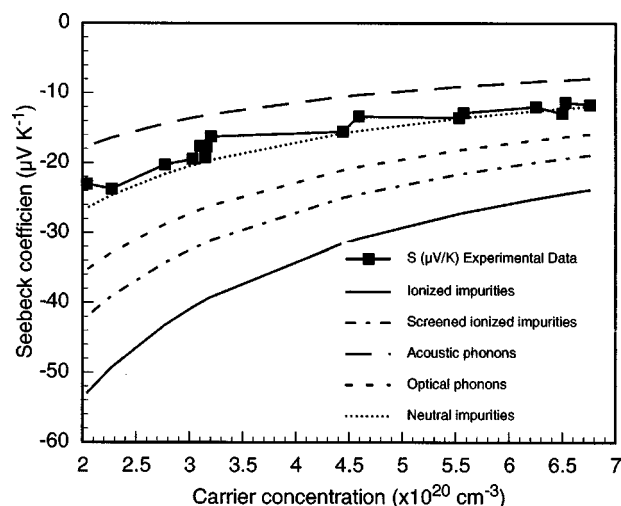


FIG. 25. Measured and modeled values of the Seebeck coefficient of  $\text{Cd}_2\text{SnO}_4$  films with carrier concentration. The various lines show the modeled variation, for various scattering mechanisms.

values for other TCOs (i.e., about  $0.3 m_e$ ), although these have not been analyzed in quite the same detail as in the present work. The unusually large mobility in  $\text{Cd}_2\text{SnO}_4$  is due to a long relaxation time rather than to a low effective mass. The long relaxation time is related to the very high-crystalline quality of the films. Using high-resolution electron microscopy, we observed lattice fringes extending across entire grains. This leads us to expect high intragrain mobility. The dominant scattering mechanisms change with carrier concentration in a similar manner to those in CdO.

Figure 25 shows the measured and modeled Seebeck coefficient as a function of carrier concentration. The scattering appears to be due to neutral impurities.<sup>2</sup> Although one may have expected ionized impurities to play a more significant role, particularly at high concentration, this does not appear to be the case. However, we stress that the range of carrier concentrations investigated is relatively limited in comparison with that of CdO. Figure 26 shows the temperature dependence of the mobility of a film with a carrier concentra-

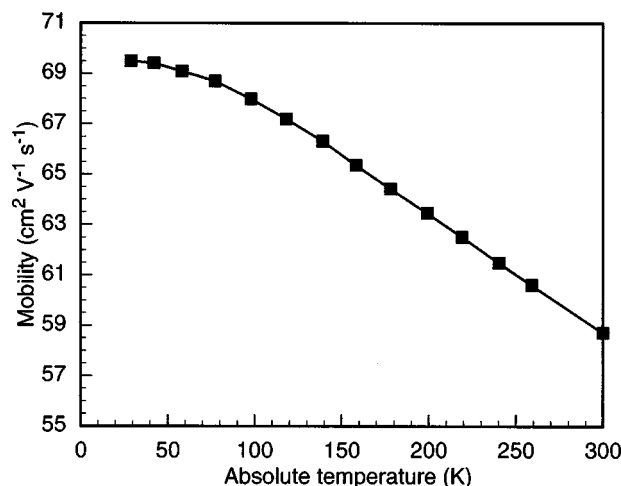


FIG. 26. Temperature dependence of the mobility of a  $\text{Cd}_2\text{SnO}_4$  film.

tion of  $4.5 \times 10^{20} \text{ cm}^{-3}$ . This is more consistent with phonon scattering. Hence, we are somewhat uncertain about the dominant scattering mechanism in these films. In addition, uncertainties in the precise shape of the conduction band may influence these conclusions.

It is interesting to consider whether grain-boundary scattering could be important. First, the mean-free path of the conduction electrons, for the very high carrier concentrations measured here, is of the order of 10 nm, i.e., much less than the size of the grains. Second, the agreement between the optical and Hall mobilities suggests that the grain boundaries play little or no role. The amplitude of vibration of electrons oscillating under the influence of the electromagnetic field is many orders of magnitude less than this. Scattering of these electrons could not, therefore, be due to the grain boundaries, but must be due to intragrain mechanisms. Third, Mulligan<sup>51</sup> suggested that the potential barrier at grain boundaries is likely to present a minimum obstacle to tunneling electrons. The height of the grain-boundary potential barrier is likely to be significantly less than the height of the Fermi level above the conduction-band minimum. Consequently, the Fermi electrons are unlikely to be scattered by the grain-boundary potential barrier.<sup>51</sup> The depletion width on either side of the grain boundary is probably on the order of 1 nm for carrier concentrations of about  $10^{20} \text{ cm}^{-3}$ , which would present a minimal obstruction to tunneling Fermi electrons. For these reasons, we do not believe that grain boundaries can be relevant to scattering of electrons in TCOs, or, perhaps, in highly degenerate semiconductors more generally.

Although we can make reasonable deductions about the nature of the scattering processes, we are unable to offer a convincing explanation of the source of the free carriers. We have applied Mössbauer spectroscopy to elucidate the location of the cations in the lattice. The indications are that the material is in the inverse form, as suggested in the literature.<sup>34,53</sup>

### C. Zinc stannate

Finally, we have analyzed  $\text{Zn}_2\text{SnO}_4$  films in greater detail than has previously been done, although these studies are still in their infancy in comparison with the other two materials discussed in this article. Unlike  $\text{CdO}$  and  $\text{Cd}_2\text{SnO}_4$ , we have not yet been able to achieve either high carrier concentration or high mobility. Although one may expect the spinel compounds to behave in a similar manner, this is clearly not the case. High-resolution transmission electron microscopy does not reveal well-oriented fringes across the width of grains, suggesting that intragrain scattering is probably stronger in  $\text{Zn}_2\text{SnO}_4$  than in  $\text{Cd}_2\text{SnO}_4$ . The carrier concentrations are much lower for the  $\text{Zn}_2\text{SnO}_4$  films studied to date, implying that their mean-free paths were longer than those in  $\text{Cd}_2\text{SnO}_4$ . Consequently, it is quite possible that grain-boundary scattering may play a greater role than is likely in a higher concentration material. As with the films of  $\text{Cd}_2\text{SnO}_4$ , we do not yet have an explanation of the source of the free carriers, although we note that their concentration is almost two orders of magnitude less than the former. We

have also found that annealing the films in air causes the carrier concentration to decrease substantially, suggesting that oxygen vacancies may be the source of the carriers.

To date, there is a tempting suggestion that the Cd-containing TCOs give a superior performance to other materials. However, this is speculation and we do not imply that we understand this idea. Future work will focus on this possibility, and we shall continue to develop and understand novel TCOs.

Note added: Since the time of presenting article, we have performed further analysis of these films. We now believe that the density-of-states effective mass is not independent of carrier concentration but increases with it. The Seebeck and Nernst coefficients were, therefore, modeled again with this knowledge and it was concluded that the main scattering mechanism was due to optical phonons, which is much easier to understand.

### ACKNOWLEDGMENTS

The authors wish to thank the many people who have helped in the execution of this work. Those at NREL include Dr. Helio Moutinho for his work on atomic-force microscopy; Dr. John Perkins for help with Raman spectroscopy; and Dr. Yanfa Yan for performing high-resolution electron microscopy. Professor Victor Kaydanov, Professor Don Williamson, and Professor Reuben Collins, of the Colorado School of Mines, all made very significant contributions. This work was supported by the U.S. Department of Energy through Contract No. DE-AC36-99GO10337. This work was originally presented as the John A. Thornton Memorial Lecture, 46th International Vacuum Symposium of the American Vacuum Society, Seattle, Washington (1999).

<sup>1</sup>T. J. Coutts, T. O. Mason, J. D. Perkins, and D. S. Ginley, in *Transparent Conducting Oxides: Status and Opportunities in Basic Research, Photovoltaics for the 21st Century*, Seattle, Washington, 1999 (The Electrochemical Society, New York, 1999), pp. 274–288.

<sup>2</sup>I. A. Rauf and J. Yuan, *Mater. Lett.* **25**, 217 (1995).

<sup>3</sup>T. J. Coutts, X. Wu, P. Sheldon, and D. H. Rose, in *Development of High-Performance Transparent Conducting Oxides and Their Impact on the Performance of CdS/CdTe Solar Cells*, 2nd World Conference on Photovoltaic Solar Energy Conversion, Vienna, Austria, 1998 (European Commission), pp. 720–723.

<sup>4</sup>G. Haacke, in *Annual Review of Materials Science*, edited by R. A. Huggins, R. H. Bube, and R. W. Roberts (Annual Reviews, Palo Alto, CA, 1977), Vol. 7, pp. 73–93.

<sup>5</sup>T. J. Coutts, X. Wu, and W. P. Mulligan, *J. Electron. Mater.* **25**, 935 (1996).

<sup>6</sup>T. J. Coutts and R. Hill, *Third International Conference on Future Energy Sources*, London, U.K. (IEE, London, 1981), pp. 147–150.

<sup>7</sup>R. D. Brown, <http://minerals.usgs.gov/minerals/pubs/commodity/indium/index.html#myb>.

<sup>8</sup>B. Andersson, in *PV and the Environment*, edited by V. Fthenakis, K. Zweibel, and P. Moskowitz (Brookhaven National Laboratory, 1998), Vol. BNL-5257.

<sup>9</sup>B. A. Andersson, C. Azar, J. Holmberg, and S. Karlsson, *Energy* **23**, 407 (1998).

<sup>10</sup>See, for example, the Web site of the U.S. Display Consortium (USDC) at <http://www.usdc.org/>. A presentation, entitled “Technical Overview of the Flat Panel Display Industry” is given by Dr. J. Norman Bardsley, Director of the USDC.

<sup>11</sup>D. K. Kramer, <http://minerals.usgs.gov/minerals/pubs/commodity/gallium/index.htm#myb>.

- <sup>12</sup>R. D. Brown, <http://minerals.usgs.gov/minerals/pubs/commodity/selenium/831399.pdf>.
- <sup>13</sup>[www.nrel.gov/ncpv](http://www.nrel.gov/ncpv), "Photovoltaic (PV) Industry Roadmap Workshop" (1999).
- <sup>14</sup>J. Plachy, <http://minerals.usgs.gov/minerals/pubs/commodity/cadmium/index.html#myb>.
- <sup>15</sup>W. Wu, P. Sheldon, T. J. Coutts, D. H. Rose, W. P. Mulligan, and H. R. Moutinho, in *NREL/SNL Photovoltaics Program Review*, edited by C. E. Witt, M. Al-Jassim, and J. M. Gee (American Institute of Physics, Lake-wood, CO, 1996), Vol. 394, pp. 693–702.
- <sup>16</sup>P. D. Moskowitz, K. Zweibel, and V. M. Fthenakis, Report No. SERI/TR-211-3261 (1990).
- <sup>17</sup>D. Bonnet and M. Harr, in "Manufacturing of CdTe Solar Cells," 2nd World Conference on Photovoltaic Solar Energy Conversion, Vienna, Austria, 1998 (European Commission), pp. 397–402.
- <sup>18</sup>X. Wu, W. P. Mulligan, and T. J. Coutts, in "Electrical and Optical Properties of Transparent Conducting Cadmium Stannate and Zinc Stan-nate Thin Films Prepared by rf Magnetron Sputtering," 39th Annual Technical Conference Proceedings of the Society of Vacuum Coaters, Philadelphia, Pennsylvania, 1996 (Society of Vacuum Coaters), pp. 217–221.
- <sup>19</sup>X. Wu, T. J. Coutts, and W. P. Mulligan, *J. Vac. Sci. Technol. A* **15**, 1057 (1997).
- <sup>20</sup>A. J. Nozik, *Phys. Rev. B* **6**, 453 (1972).
- <sup>21</sup>F. P. Koffyberg and F. A. Benko, *Appl. Phys. Lett.* **37**, 320 (1980).
- <sup>22</sup>E. Leja, T. Stapinski, and K. Marszalek, *Thin Solid Films* **125**, 119 (1985).
- <sup>23</sup>T. Pisarkiewicz, K. Zakrzewska, and E. Leja, *Thin Solid Films* **153**, 479 (1987).
- <sup>24</sup>M. T. Mohammad and W. A. S. A. Ghafor, *Solid State Commun.* **88**, 227 (1993).
- <sup>25</sup>Y. Dou and R. G. Egdell, *Surf. Sci.* **372**, 289 (1997).
- <sup>26</sup>H. Enoki, T. Nakayama, and J. Echigoya, *Phys. Status Solidi A* **129**, 181 (1992).
- <sup>27</sup>X. Wu, P. Sheldon, Y. Mahathongdy, R. Ribelin, A. Mason, H. R. Moutinho, and T. J. Coutts, Report No. NREL/CP-520-25656 (1998).
- <sup>28</sup>D. H. Zhang and H. L. Ma, *Appl. Phys. A: Mater. Sci. Process.* **62**, 487 (1996).
- <sup>29</sup>H. Kawazoe, M. Yasukawa, H. Hyodo, M. Kurita, H. Yanagi, and H. Hosono, *Nature (London)* **389**, 939 (1997).
- <sup>30</sup>A. Kudo, H. Yanagi, K. Ueda, H. Hosono, H. Kawazoe, and Y. Yano, *Appl. Phys. Lett.* **75**, 2851 (1999).
- <sup>31</sup>D. R. Kammler, D. D. Edwards, B. J. Ingram, T. O. Mason, G. B. Palmer, A. Ambrosine, and K. R. Poeppelmeier, in *The 195th Meeting of the Electrochemical Society—Photovoltaics for the 21st Century*, Seattle, WA, edited by V. K. Kapur, R. D. McConnell, D. Carlson, G. P. Ceaser, and A. Rohatgi (The Electrochemical Society, Pennington, NJ, 1999), Vol. 99-11, pp. 68–77.
- <sup>32</sup>X. Wu, P. Sheldon, Y. Mahathongdy, R. Ribelin, A. Mason, H. R. Moutinho, and T. J. Coutts, in "CdS/CdTe Thin-Film Solar Cell with a Zinc Stannate Buffer Layer," *NCPV Photovoltaics Program Review—Proceedings of the 15th Conference*, Denver, CO (AIP, Woodbury, NY, 1998), pp. 37–41.
- <sup>33</sup>X. Li, T. A. Gessert, P. Sheldon, and R. Ribelin, *J. Vac. Sci. Technol.* (to be published).
- <sup>34</sup>N. V. Porotnikov, V. G. Savenko, and O. V. Sidorova, *Russ. J. Inorg. Chem.* **28**, 932 (1983).
- <sup>35</sup>N. Yamada, Y. Yasui, H. Li, Y. Ujihara, and K. Nomura, *Jpn. J. Appl. Phys., Part 1* **38**, 2856 (1999).
- <sup>36</sup>D. L. Williamson, *Hyperfine Interact.* **40**, 249 (1988).
- <sup>37</sup>W. Schiessl, W. Potzel, H. Karzel, C. Schäfer, M. Steiner, M. Peter, G. M. Kalvius, I. Halevy, J. Gal, W. Schäfer, and G. Will, *Hyperfine Interact.* **68**, 161 (1991).
- <sup>38</sup>V. I. Kaidanov and I. A. Chernik, *Sov. Phys. Solid State* **1**, 1159 (1967).
- <sup>39</sup>M. K. Zhitinskaya, V. I. Kaidanov, and I. A. Chernik, *Sov. Phys. Solid State* **8**, 246 (1966).
- <sup>40</sup>J. Kolodziejczak and L. Sosnowski, *Phys. Status Solidi* **1**, 399 (1962).
- <sup>41</sup>D. L. Young, T. J. Coutts, V. I. Kaydanov, and W. P. Mulligan, *J. Vac. Sci. Technol.* (to be published).
- <sup>42</sup>D. L. Young, T. J. Coutts, and V. I. Kaydanov, *Rev. Sci. Instrum.* **71**, 462 (2000).
- <sup>43</sup>J. Kolodziejczak and S. Zukotynski, *Phys. Status Solidi* **5**, 145 (1964).
- <sup>44</sup>X. Wu, W. P. Mulligan, and T. J. Coutts, *Thin Solid Films* **286**, 274 (1996).
- <sup>45</sup>K. Gurumurugan, D. Mangalaraj, and S. K. Narayandass, *J. Electron. Mater.* **25**, 765 (1996).
- <sup>46</sup>F. P. Koffyberg, *Solid State Commun.* **9**, 2187 (1971).
- <sup>47</sup>F. P. Koffyberg, *Can. J. Phys.* **49**, 435 (1971).
- <sup>48</sup>H. Finkenrath, H. Köhler, and M. Lochmann, *Z. Angew. Phys.* **21**, 512 (1966).
- <sup>49</sup>L. A. Siegel, *J. Appl. Crystallogr.* **11**, 284 (1978).
- <sup>50</sup>R. Wyckoff and W. G., *Crystal Structures* (Interscience, New York, 1968), Vol. 4.
- <sup>51</sup>W. P. Mulligan, Ph.D. thesis, Colorado School of Mines (1997).
- <sup>52</sup>R. D. Shannon, *Acta Crystallogr., Sect. A: Cryst. Phys., Diff., Theor. Gen. Crystallogr.* **A32**, 751 (1976).
- <sup>53</sup>R. H. Hill, J. R. Craig, and G. V. Gibbs, *Phys. Chem. Mater.* **4**, 317 (1979).